Int J Adv Manuf Technol (2009) 44:255–264
DOI 10.1007/s00170-008-1832-7

ORIGINAL ARTICLE

Numerical analysis for effect of process parameters of low-current micro-PAW on constricted arc

Pei-quan Xu · Shun Yao · Jian-ping He · Chun-wei Ma · Jiang-wei Ren

Received: 17 August 2008 / Accepted: 31 October 2008 / Published online: 21 November 2008

Abstract A model was put forward to simulate the electromagnetic phenomena and fluid field in plasma arc occurring during the low-current microplasma arc welding (low-current micro-PAW) process. The effects of the nozzle neck-in and welding current of micro-plasma arc on the arc electromagnetic field distribution were discussed. Finally, under the condition of different welding current, welding voltage, arc length, shield gas flow rate, and plasma flow rate, welding experiments of image sampling were carried out. Three types of microplasma arc, namely, needle plasma arc, columnar plasma arc, and opening model plasma arc, are founded by experiment. Based on the unified model, a thorough investigation of the low-current microplasma arc characteristics during the micro-PAW process was conducted. It was found that the process parameters have significant effects on the microplasma arc and the distributions of current density and electromagnet force distribution.

Keywords Low current micro-PAW · Numerical simulation · Current density · Electromagnet force

P.-q. Xu (✉) · J.-p. He · C.-w. Ma · J.-w. Ren
School of Materials Engineering,
Shanghai University of Engineering Science,
Shanghai 201620, China
e-mail: xupeiquan7810@yahoo.com.cn

S. Yao
School of Materials Science and Engineering,
Shanghai Jiao Tong University,
Shanghai 200240, China
e-mail: ys@sjtu.edu.cn

1 Introduction

Low-current micro-PAW process is usually used for joining fabrication of thin metal foil. During micro-PAW process, the effects of heat and force on welded joint can be divided into two parts: the arc plasma and the welding pool induced by arc plasma. Wherein, heat transfer is mainly caused by ionization reaction and electromagnetic field action from arc plasma, and the forces include gravity, surface tension, electromagnetic force, arc pressure, and plasma shear stress [1].

Therefore, arc appearance investigation is significant to the formation mechanism of welding pool and welding quality control. The major arc constriction mechanism is as follows:

1. Thermo constriction effect

Solids expand as the temperature increases and contract when they are cooled. Therefore, while the plasma body flows through the nozzle, cooled by copper cooling stave, the thermal difference constricted the plasma arc.

2. Electromagnetic constriction effect

While plasma leads to a certain direction driven by the current, it can be looked as conductor. According to the electromagnetic theory, forces on a current-carrying conductor affected by the adjacent conductors constrict the plasma arc.

3. Mechanical constriction effect by constricted nozzle and copper stave

While plasma flows through the nozzle chamber (copper cooling stave) and exit area of nozzle with size of 1 mm or so, the plasma is constricted by constricted nozzle and

copper cooling stave. Micro-PAW features a constricted arc between a non-consumable electrode and the weld pool or between the electrode and the constricting nozzle (non-transferred arc).

4. Constriction effect by impulse current

Under the optimum condition, impulse current density is approximately twice higher than that with continuous current density during plasma welding process. Moreover, under the low current with high frequency, the effect is more significant.

The complex welding process not only includes multi-field coupling, such as electromagnetic field, flow field, temperature field, etc., but also requires the nonlinear solution for the proposed model. The problem of simulating the welding process may be treated as a non-linear programming problem and confirmed via real experiment. Therefore, thermo, power, and flow mechanism during welding process have called more and more eyes from all of the worlds. Numerical simulations based on welding arc and weld pool are the two important research direction on welding mechanism simulation. At present, numerical simulation on projection welding, friction stir welding, plasma arc forming, tungsten inert gas welding, and gas metal arc welding process have been studied [2–6]. Three-dimensional, transient simulations of the plasma flow inside different plasma spray torches have been performed using a local thermodynamic equilibrium (LTE) model solved by a multiscale finite-element method [5].

Using low current, Messaad et al. [7] developed a numerical model describing the arc-cathode region. In this study, the arc is treated as a steady-state phenomenon. The model is then applied to a vacuum arc discharge interacting with a Cu cathode at low current of 4–50 A. Basic heat source properties of argon hollow cathode arc at the atmospheric pressure are numerically analyzed to improve the heat concentration in low pressure [8]. According to temperature distributions and history in double-sided arc weldment, Prof. Wu et al. developed a numerical model; thus, the temperature distributions and profiles at different cross-sections and along different lines of interest could be computed [9, 10]. From the numerical analysis and experimental, the effect of plasma appearance on temperature field, arc force, and welding residual stress is significant. On this basis, the coupled simulation of arc and welding pool could be built [11–13].

However, the research of numerical simulation on welding process is less related to micro-PAW, especially the low-current micro-PAW process. In this paper, on the analysis of constriction mechanism, coupled field numerical model with temperature field, electromagnetic field, and flow field is investigated based on low-current micro-PAW and thin metal foil welding. The experimental architecture, procedures, and the process parameters used in micro-PAW process are established in Section 2. In Section 3, we present a numerical model and its boundary conditions. The numerical results is illustrated in Section 4 and then confirmed by real experimental. The effects and influence factors are discussed in Section 5, and conclusion is drawn in Section 6.

2 Micro-PAW equipment and welding parameters

Figure 1 illustrates overall architecture of micro-PAW equipment; this platform includes welding torch, traveling car, micro-PAW machine, control panel, and subsidiary body. In order to obtain a very stable, controllable arc for joining fine sheet down to 0.1-mm thickness under the low current.

The equipment and its facilities include:

1. Micro-PAW welder based on digital signal processor (DSP) control system. The stable welding current is 0.08–30 A. Current fluctuation is less than 0.1 A; impulse frequency is 1–500 Hz
2. Welding traveler and control unit
3. Clamping fixture

Welding parameters are illustrated in Table 1, which consist of welding current, welding voltage, electrode diameter, nozzle diameter, shielding gas flow L_1, and plasma gas flow L_2. Materials to be welded is stainless steel, which chemical composition is, 0.08%C, 1.00%Si, 2.00%Mn, 0.045%P, 0.03%S, 8.0–10.5%Ni, 18.0–20.0% Cr, and Fe(Bal.).

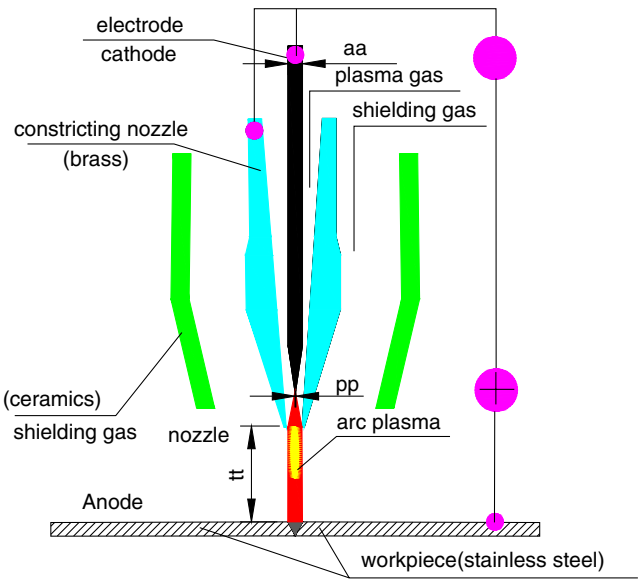

Fig. 1 Architecture of the micro-PAW process

Table 1 Welding parameters during micro-PAW process

Arc length L_0 (mm)	Nozzle neck-in *tttt* (mm)	Welding current I (A)	Welding voltage U (V)	Plasma gas flow L_1 (L/min)	Shielding gas flow L_2 (L/min)
3–7	0.5–2.5	0.8–15	15–30	0.5–1	3–7

3 Mathematical model

Figure 2 is a schematic sketch of a stationary axisymmetric constriction model in micro-PAW system. In this model, current is applied to the electrode through the contact tube. A microplasma arc generated between the electrode and the workpiece and weld pool with surface depression is formed by dynamic interaction with the high-temperature and high-pressure arc plasma at the workpiece. Inert shielding gas is provided through the shielding gas nozzle to prevent the weld metal from oxidation.

3.1 Assumptions

The assumptions of micro-PAW arc based on constricted arc and low current are given:

1. The whole welding arc is axial symmetric.
2. The arc plasma is LTE.
3. The plasma is turbulent and compressible.
4. The effect of weld pool on arc appearance is omitted.

3.2 Governing equation

The single-stage constriction micro-PAW has an anode region, an arc region, and a cathode region. The anode region is the electrode, and the cathode region is the workpiece. The anode sheath region and the cathode sheath region have been omitted and treated as special boundary conditions in this model for computational simplification [7, 8]. The differential equations governing the conservation of mass, momentum, and energy based on the continuum formulation and constricted arc are employed in the present study. The current continuity equation is used to calculate the current density distribution. The mass continuity equations are divided two parts.

While the plasma arc flows through constricted nozzle (IH, $z\in[tt,tt+tttt]$), in this region, the arc is constricted by mechanical constriction, thermal constriction and electromagnetic constriction, high frequency constriction, and the mass continuity equation can be given as follows:

$$\rho u \mathrm{d}A = \text{const} \tag{1}$$

Where ρ is mass density, u is the plasma arc velocity while flowing through constricted nozzle, A is the area of cross-section, which plasma arc flows through.

If the above parameters are evenly distributed, on the cross-section, Eq. 1 can be given:

$$\frac{\mathrm{d}\rho}{\rho}+\frac{\mathrm{d}u}{u}+\frac{\mathrm{d}A}{A}=0 \tag{2}$$

While the plasma arc flows until workpiece surface (FG, $z\in[0,tt]$), the mass continuity equation is given as follows:

$$\frac{\partial}{\partial t}(\rho)+\nabla\cdot(\rho V)=0 \tag{3}$$

Momentum equation

$$\begin{aligned}&\frac{\partial}{\partial t}(\rho u)+\nabla\cdot(\rho V u)=\nabla\cdot\left(\mu_1\frac{\rho}{\rho_1}\nabla u\right)\\&-\frac{\partial p}{\partial r}-\frac{\mu_1}{K}\frac{\rho}{\rho_1}(u-u_s)\\&-K-\nabla\cdot(\rho f_s f_1 V u)-J_z\times B_\theta\end{aligned} \tag{4}$$

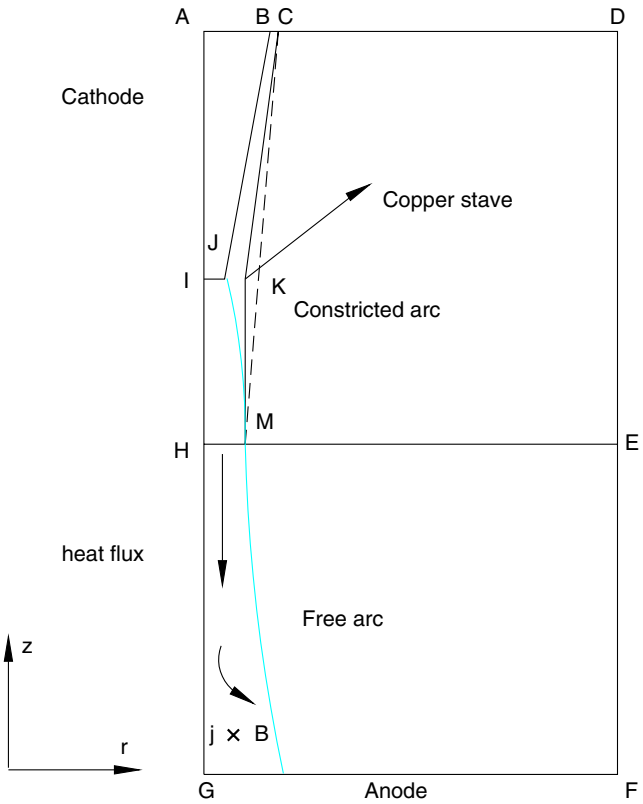

Fig. 2 Constricted-arc appearance model of micro-PAW

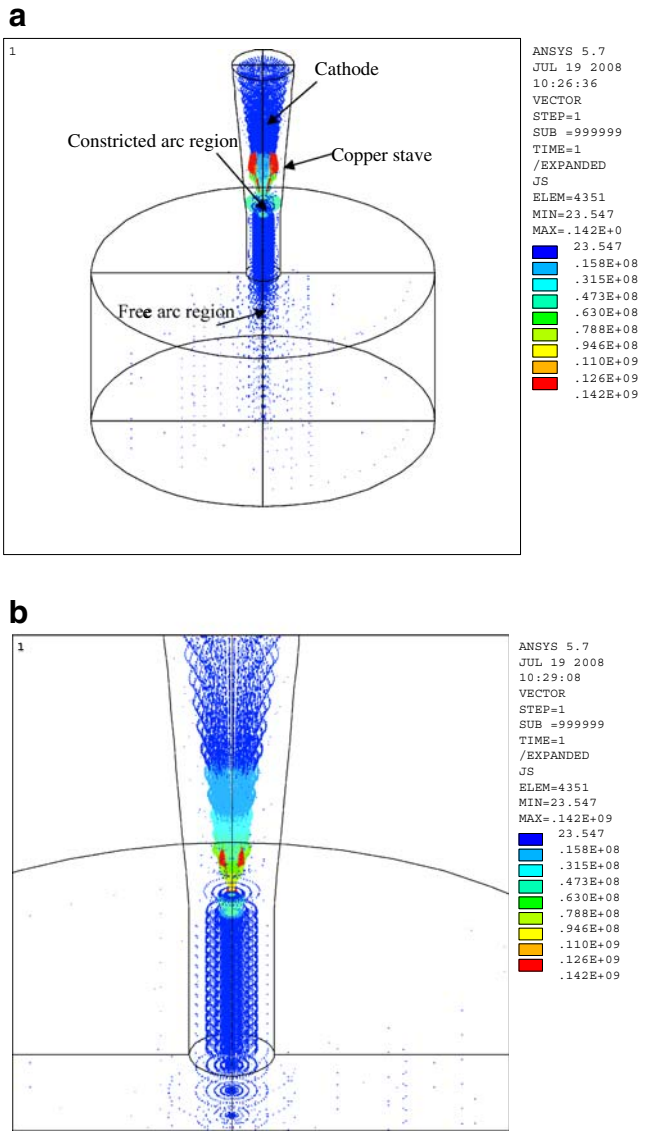

Fig. 3 Current density distribution. **a** The whole proposed model; **b** the constricted arc region

While the plasma gas is compressible, the energy conservation equation is given by:

$$\int \frac{dp}{\rho} + \frac{u^2}{2} = C^{\frac{1}{k}} \int \rho^{-\frac{1}{k}} d\rho + \frac{u^2}{2} = \frac{p}{\rho} + \frac{u_z^2}{2} + \frac{RT}{k-1} \qquad (5)$$

Where, T is temperature, $C = \frac{p}{\rho^k}$

While welding current flows through the micro-PAW arc region, the electromagnetic equations are required to get electromagnetic force and the joule heat. Consequently, the electromagnetic force and the joule heat can be transferred to arc fluid field analysis.

The general equations and the link equation between the electromagnetic equations and the plasma fluid equations are given as follows.

The electromagnetic equations are given in MKS units because the magnetic field is usually described in terms of Gauss, 1 T=10^4 G. Maxwell's equations are

$$\nabla \times B = \mu_0 j + 1/c^2 \cdot \partial E/\partial t \qquad (6)$$

where the last term on the right-hand side is the displacement current.

B	is referred to as the magnetic field (the magnetic induction) or self-induced magnetic field
$\mu_0 = 4\pi \times 10^{-7}$ H/m	is the magnetic permeability in a vacuum
J	is the current density, here, j_x and j_z are radial and axial current

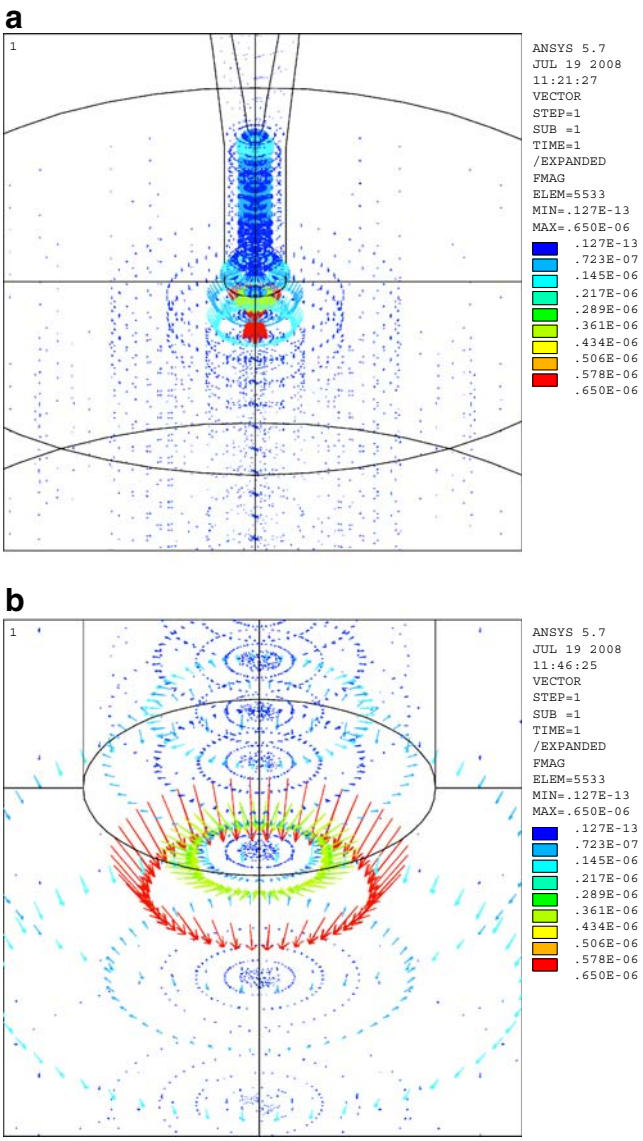

Fig. 4 Electromagnet force distribution. (**a**) The arc region; (**b**) cathode region

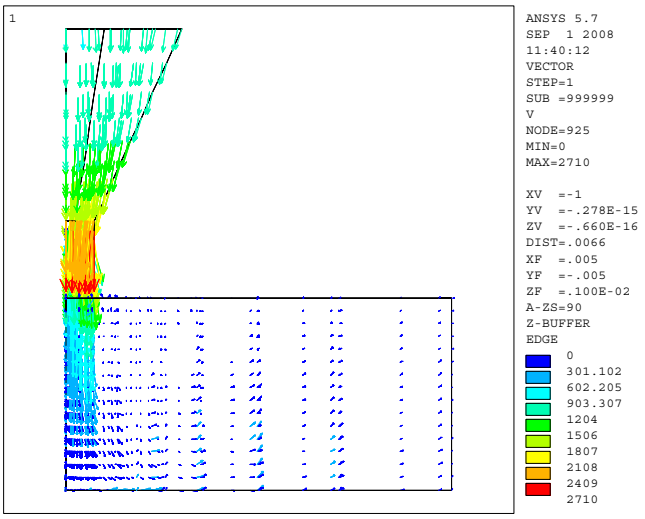

Fig. 5 Flow velocity distribution

density, respectively, according to Ohm law:

$$j_x = -\sigma \frac{\partial \phi}{\partial x},\ j_z = -\sigma \frac{\partial \phi}{\partial z} \tag{7}$$

E is the electric field

c is the speed of light in a vacuum, $c = (\mu \cdot \varsigma)^{-1/2} \approx 3 \times 10^8$ m/s

ς is the permittivity of free space

According to Faraday's law of magnetic induction with

$$\nabla \times E = -\partial B/\partial t \tag{8}$$

This indicates that a spatially varying electric field can induce a magnetic field.Assume that the typical length scale for plasma variations is L and that typical timescales are of order T.

Two quantities can be used to define a typical plasma velocity as $V = L/T$.The displacement current is

$$\frac{1}{c^2} \cdot \frac{\partial E}{\partial t} \approx \frac{1}{c^2} \cdot \frac{E}{T} = \frac{V}{c^2} \cdot \frac{B}{T} = \frac{B}{L} \cdot \frac{V^2}{c^2} \tag{9}$$

Hence, if the typical plasma velocities satisfy $V^2 << c^2$, then the displacement current is much smaller than $\nabla \times B$. This is the MHD approximation, so that Ampere's law simplifies to

$$\nabla \times B = \mu \cdot j \tag{10}$$

By assuming the plasma obeys charge neutrality, the final electromagnetic equation is Ohm's law:

$$j = \sigma(E + v \times B) \tag{11}$$

Where σ is the electrical conductivity in mho/m. This is effectively a generalization of the simple $U=I$ times resistance to a moving conductor. ν is the plasma velocity, and it is Ohm's law that provides the link between the electromagnetic equations and the plasma fluid equations.

Plasma gas and welding shield gas is argon. Thermophysical properties of argon are given in [10, 13].

3.3 Boundary conditions

Within the computational domain, such boundaries as temperature, velocity, or electrical potential are added to the area as follows:

IG boundary

$$u_r = 0;\ \partial u_z/\partial r = 0;\ \partial \phi/\partial r = 0;\ \partial T/\partial r = 0;$$

GF boundary

$$u_r = 0;\ u_z = 0;\ u_\theta = 0;\ \phi = 0;\ \mathrm{T} = 5000\ \mathrm{K}$$

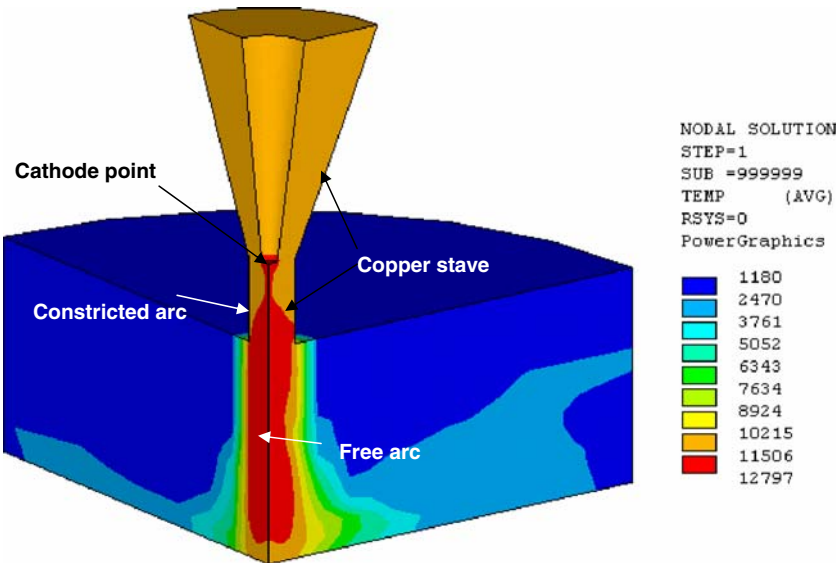

Fig. 6 Constricted arc appearance of micro-PAW by numerical simulation (I=0.8 A, U=30 V; L_1=0.5 L/min, L_2=5 L/min, L_0=5 mm)

FD boundary

$u_r = 0;\ u_z = 0;\ u_\theta = 0;\ \partial\phi/\partial r = 0;$

DB boundary

$u_r = 0;\ u_z = u_{\text{gas}};\ \partial\phi/\partial z = 0;\ \text{T} = 1000\ \text{K}$

BJ, IJ boundary

$u_r = 0;\ u_z = 0;\ u_\theta = 0;\ \text{T} = 3000\ \text{K}$

AB boundary

$j_z = I/\pi r_0^2$

CM (CKM) boundary

$u_r = 0;\ u_z = 0;\ u_\theta = 0;\ \phi = 0;$

T=293 K

Initial temperature of boundary GF is 5,000 K, which is determined by excitation temperature of plasma body between anode and cathode abide by material properties; thus, the plasma body can be excited. In our algorithm, we specified the boundary condition by setting excitation temperature for plasma gas so that the gas can be ionized. During the calculation, the load "temperature" for second, third, …iteration calculation is read from fluid calculation results.

4 Results

4.1 Current density distribution

Current density vector distribution of arc region (including constricted arc and free arc) is shown in Fig. 3. The current density distribution for the whole proposed model is illustrated in Fig. 3a; Fig. 3b addresses the current density distribution in the constricted arc region. The results manifest that current density achieves the highest value at cathode spot for its small area. In constricted arc region, the current density is of uniform size and direction, and current density becomes larger with axial distance nearing to the cathode. Current density decreases with radial distance increasing. It is known that arc conductivity of argon gas and electric conductivity affect current density distribution of welding arc directly.

4.2 Electromagnet force distribution

Electromagnet force is one of the most important forces to drive the plasma arc to workpiece. After the magnetic field analysis, the electromagnet force distribution for the plasma arc region is illustrated in Fig. 4a, and electromagnet force distribution for cathode region is illustrated in Fig. 4b.

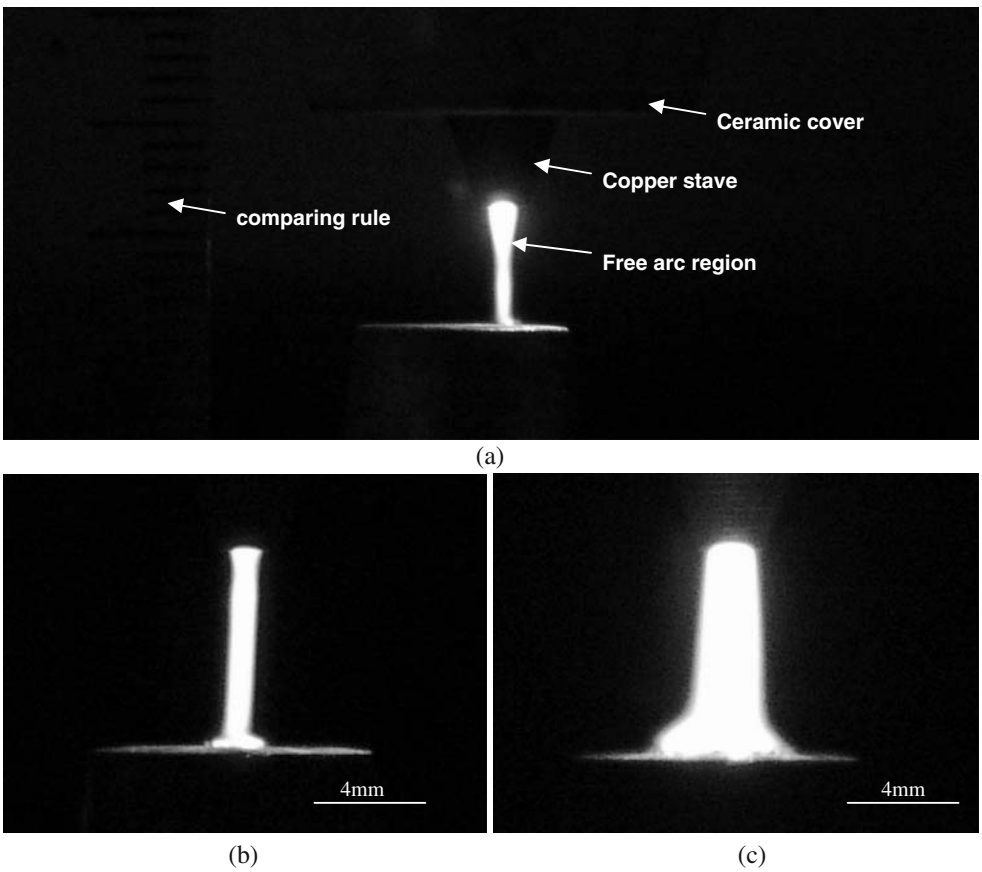

Fig. 7 Constricted arc appearance of microplasma arc under different welding parameters. **a** I=0.8A, U=30 V, L_1=0.5 L/min, L_2=5 L/min, L_0=5 mm; **b** I=0.8 A, U=28 V, L_1=0.5 L/min, L_2=7 L/min, L_0=7 mm; **c** I=3.5 A, U=26 V, L_1=0.5 L/min, L_2=7 L/min, L_0=7 mm

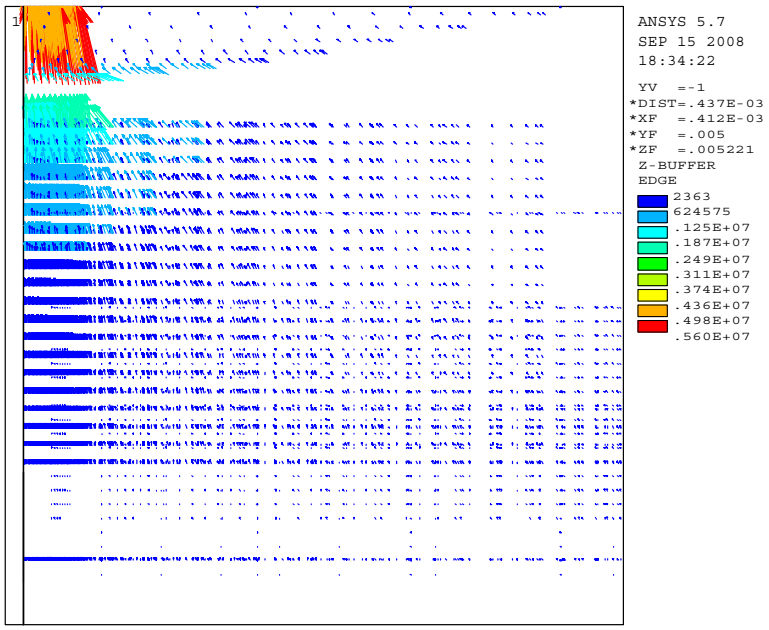

(a) tttt=0.5mm

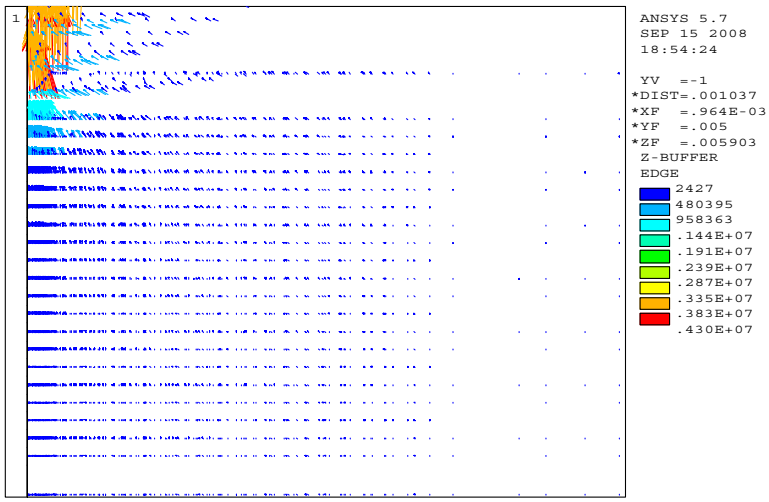

(b) tttt=1.5mm

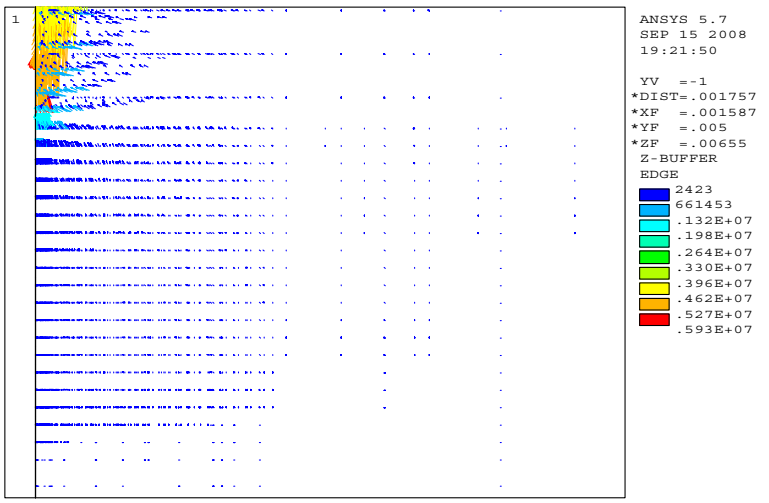

(c) tttt=2.5mm

Fig. 8 Effect of neck-in of welding gun on current density distribution. **a** *tttt*=0.5 mm. **b** *tttt*=1.5 mm. **c** *tttt*=2.5 mm

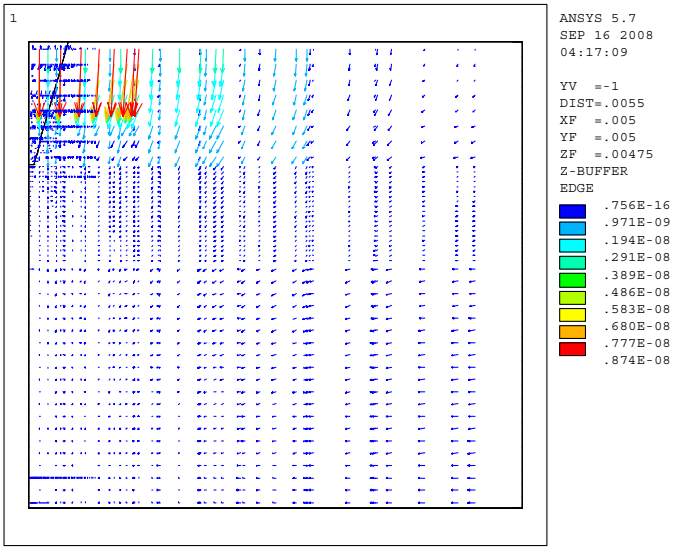

(a) currentpl = 5A

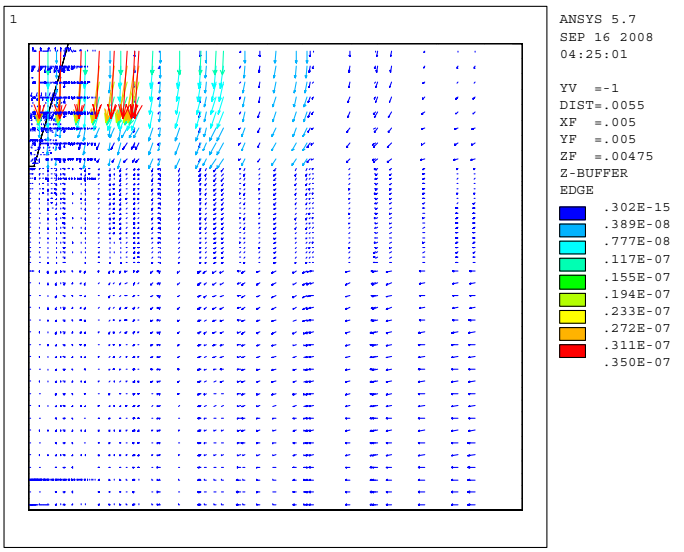

(b) currentpl = 10A

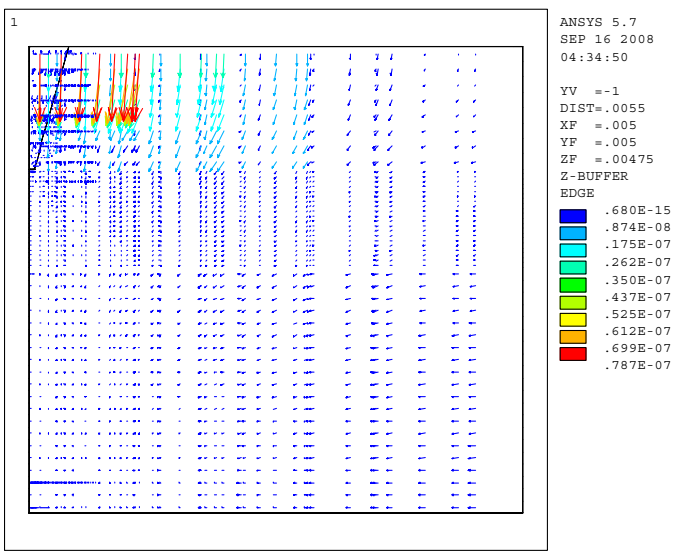

(c) currentpl = 15A

Fig. 9 Effect of welding current on electromagnet force. **a** currentpl=5 A. **b** currentpl=10 A. **c** currentpl=15 A

From the above results, the electromagnet force distributes from cathode spot to workpiece surface and achieves the highest value at outlet of nozzle region. This is because of the constricted effects by copper stave.

4.3 Flow velocity distribution

Plasma flow field describe the plasma flow velocity in different position; from it, we disclose the flow velocity distribution. On the basis of current density analysis and electromagnet force distribute analysis, the plasma flow field is shown in Fig. 5.

From the plasma flow distribution graph, in constriction stage, the plasma velocity is approximately 2,710 m/s; in free arc region, the plasma velocity is 903 m/s or so, and in near workpiece surface, the plasma velocity is 301 m/s. In the model axial cord, the most velocity is achieved; with the increase of the distance to axial cord, the velocity decreases accordingly.

4.4 Plasma arc appearance

In order to simulate the plasma arc appearance, temperature field distribution is used to describe the arc appearance. While I=0.8 A, U=28 V, L_1=0.5 L/min, L_2=7 L/min, L_0=7 mm, constricted arc appearance of micro-PAW by numerical simulation is shown in Fig. 6. From the results, we can see that the appearance manifests the columnar shape and in temperature range 1,180 to 12,797 K.

4.5 Arc appearance experimental results

Using welding parameters proposed in Section 2, different plasma arc appearances are addressed using an image-processing experiment, and the results are shown in Fig. 7. From the image, we can see that the free arc column comes into being during the nozzle outlet and workpiece with three typical arc appearances under different welding parameters. Actually, the constricted arc comes into being in the nozzle region.

5 Discussion

We address the effect of nozzle neck-in of plasma welding gun on the current density distribution. The results are illustrated in Fig. 8, wherein Fig. 8a illustrates the current density distribution while the nozzle neck-in *tttt* is equal to 0.5 mm; Fig. 8b illustrates the current density distribution while the nozzle neck-in *tttt* is equal to 1.5 mm; and Fig. 8c illustrates the current density distribution while the nozzle neck-in *tttt* is equal to 2.5 mm.

By contrast, current density reaches the lower range value 2,427 A/m^2 while the nozzle neck-in *tttt* is 1.5 mm, which distribute in the free arc region; while the nozzle neck-in *tttt* is equal to 2.5 mm, current density reaches the higher range value 5.93×10^6 A/m^2. The direction is from workpiece surface to anode region, and with the increase of nozzle neck-in, the scope of current density distributes widely.

Consequently, we investigated the effect of welding current of plasma welding on the electromagnet force distribution. The results are illustrated in Fig. 9, wherein Fig. 9a illustrates the electromagnet force distribution while the welding current currentpl is equal to 5 A; Fig. 9b illustrates the electromagnet force distribution while the welding current currentpl is equal to 10 A; and Fig. 9c illustrates the electromagnet force distribution while the welding current currentpl is equal to 15 A. Electromagnet force near cathode region reaches the higher value, and with increase of welding current, the electromagnet force increase. The direction of electromagnet force abides by the left-hand rule.

6 Conclusions

1. Using proposed numerical simulation model, current density distribution and electromagnet force distribution are revealed. With the increase of nozzle neck-in, the scope of current density distributes widely. Electromagnet force near cathode region reaches the higher value, and with increase of welding current, the electromagnet force increase.
2. While I=0.8 A, U=28 V, L_1=0.5 L/min, L_2=7 L/min, L_0=7 mm, the constricted plasma arc appearance manifests columnar shape.

Acknowledgments The authors acknowledge the support of Shanghai Educational Development Foundation (2008cg62), specialized funds from Shanghai Municipal Education Commission (06zz79), Specialized Research Fund for Excellent Young Teachers of Shanghai (06xpyq17), the Scientific Program of Science & Technology department of Shanghai (061111034) and many thanks will be given to Dr. Lu F G, Professor Tang X H from Shanghai Jiao Tong University and W. Zhang from Shanghai Laser Manufacturing Institute.

References

1. Hu J, Tsai HL (2007) Heat and mass transfer in gas metal arc welding. Part I: The arc. Int J Heat Mass Transfer 50:833–846. doi:10.1016/j.ijheatmasstransfer.2006.08.025
2. Zhu WF, Lin ZQ, Lai XM, Luo AH (2006) Numerical analysis of projection welding on auto-body sheet metal using a coupled

finite element method. Int J Adv Manuf Technol 28:45–52. doi:10.1007/s00170-004-2336-8
3. Zhang Z, Zhang HW (2008) A fully coupled thermo-mechanical model of friction stir welding. Int J Adv Manuf Technol 37:279–293. doi:10.1007/s00170-007-0971-6
4. Xu WJ, Fang JC, Wang XY, Wang T, Liu F, Zhao ZY (2005) A numerical simulation of temperature field in plasma-arc forming of sheet metal. J Mater Process Technol 164–165:1644–1649. doi:10.1016/j.jmatprotec.2005.01.007
5. Trelles JP, Heberlein JR (2006) Simulation results of arc behavior in different plasma spray torches. J Therm Spray Techn 15:563–569. doi:10.1361/105996306X147252
6. Schnick M, Fussel U, Zschetzsche J, Guth U, Zosel J (2005) Measurement and simulation of plasma and shielding gas flows in welding arcs. Weld World 49:413–417
7. Messaad M, Belarbi AW, Abbaoui M, Lefort A (2007) A simple model for the interaction of a low-current vacuum arc with a copper cathode. J Eng Phys Thermophysics 80:1130–1139. doi:10.1007/s10891-007-0146-1
8. Tashiro S, Tanaka M, Nakatani M, Tani K, Furubayashi M (2007) Numerical analysis of energy source properties of hollow cathode arc. Surf Coat Tech 9–11:5431–5434. doi:10.1016/j.surfcoat.2006.07.158
9. Wu CS, Sun JS (2002) Numerical analysis of temperature field during double-sided arc welding of thick materials. Comput Mater Sci 25:457–468. doi:10.1016/S0927-0256(02)00323-3
10. Lu FG, Tang XH, Yu HL, Yao S (2006) Numerical simulation on interaction between TIG welding arc and weld pool. Comput Mater Sci 35:458–465. doi:10.1016/j.commatsci.2005.03.014
11. Peters J, Bartlett B, Lindsay J, Heberlein J (2008) Relating spectroscopic measurements in a plasma cutting torch to cutting performance. Plasma Chem Plasma Process 28:331–352. doi:10.1007/s11090-008-9129-z
12. Foest R, Schmidt M, Becker K (2006) Review Microplasmas, an emerging field of low- temperature plasma science and technology. Int J Mass Spectrom 248:87–102. doi:10.1016/j.ijms.2005.11.010
13. Choo RTC, Szekely J, David SA (1992) On the calculation of the free surface temperature of gas-tungsten-arc weld pools from first principles. II: Modeling the weld pool and comparison with experiments. Metall Trans B 23:371–384